Chinese Chemical Letters 36 (2025) 110292

Contents lists available at ScienceDirect

Chinese Chemical Letters

journal homepage: www.elsevier.com/locate/cclet

Robust free-base and metalated corrole radicals with reduction-induced emission

Pengfei Li[a], Chulin Qu[a], Fan Wu[a,b,*], Hu Gao[a,c], Chengyan Zhao[a], Yue Zhao[a], Zhen Shen[a,*]

[a] State Key Laboratory of Coordination Chemistry, Collaborative Innovation Center of Advanced Microstructures, School of Chemistry and Chemical Engineering, Nanjing University, Nanjing 210023, China
[b] School of Chemistry and Materials Science, Nanjing Normal University, Nanjing 210023, China
[c] College of Materials Science and Engineering, Nanjing Forestry University, Nanjing 210037, China

ARTICLE INFO

Article history:
Received 23 May 2024
Revised 14 July 2024
Accepted 23 July 2024
Available online 23 July 2024

Keywords:
Radicals
Porphyrinoids
Macrocyclic ligands
Luminescence
Redox chemistry

ABSTRACT

Preparing free-base porphyrinoid radicals that can function as coordination ligands is a challenging task. Here we report the synthesis of a stable, free-base benzocorrole (**BC**) radical containing only two inner NH protons *via* a *retro*-Diels-Alder conversion. The radical character of **BC** was fully supported by crystallographic analysis, spectroscopic evidence, and theoretical calculations. This neutral radical ligand allowed easy insertion of Zn(II), Ga(III), and Pd(II) ions to produce radical complexes. All these radicals exhibited luminescence-on responses under weak reducing atmosphere, corresponding to the conversion to their aromatic anions. The red fluorescence was observed for **BC** and its Zn(II) and Ga(III) complexes, and the near-infrared phosphorescence (>900 nm) was detected for Pd(II) complex at room temperature. Furthermore, Ga(III) corrole exhibited a variation in fluorescence in response to axial coordination. Our findings provide a promising radical platform for coordination and developing novel functional materials with switchable spin and emission.

Organic radicals have attracted considerable interest in various application fields because of their distinct redox and magnetic properties offered by the unpaired electrons [1-3]. However, the active nature of radicals makes their synthesis and manipulation very challenging. Porphyrinoids are typically aromatic macrocycles with $[4n+2]$ π-conjugation systems (*e.g.*, 18 π tetrapyrrolic porphyrin, corrole, and phthalocyanine) (Fig. 1a). The redox activity of porphyrinoids enables the generation of $[4n+1]/[4n+3]$ π radical ions *via* one-electron redox reactions. The porphyrinoid radicals could be stabilized *via* spin delocalization on their large π-conjugated systems [4], but most of them only exist in their coordinated forms with the insertion of boron [5,6], phosphorus [7], and various metal ions [8-10]. The absence of free amines in coordinated porphyrins allows for easier radical stabilization. The direct redox reactions on free-base porphyrins usually involve complicated deprotonation-protonation processes and other side reactions [11-13], making the identification and isolation of desired radicals extremely difficult. Free-base porphyrinoid radicals are assumed to be flexible, sensitive to outer stimulus, and easy to be functionalized *via* coordination, but reports of such molecules are still rare [14-18] .

Corroles are one-carbon-short porphyrins that typically have three inner NHs in their free-base forms. The electron-rich nature and squeezed inner cavity of corrole provide non-innocent coordination properties for sustaining radicals [19]. When coordinated with some metal ions such as Cu(II), Ni(II), and Pt(IV) [20-23], corroles could undergo ring-oxidation to function as dianion radical ligands. The unique coordination performances of corroles lead to a wide range of diversified applications including biomedical theranostics [24-26], catalysis [27-33], and spintronics [34-37]. Benzofusion is a highly effective method for raising the energy of the π HOMO of corrole and regulating the D-π interaction between the corrole ligand and the central ion. Paolesse and co-workers reported the first free-base tetrabenzocorrole *via* a cross-coupling method, which is a 3NH closed-shell molecule bearing eight peripheral -CO_2CH_3 groups. In addition, they have effectively synthesized a variety of benzocorrole complexes with the insertion of Cu, Co, Sn and Al ions [38,39]. We also successfully synthesized Cu(II) and Ni(II) benzocorrole complexes that were metalated using one-pot procedures. These complexes demonstrated intriguing capabilities in sustaining stable π-radicals and have been employed in the study of spin modulation [34,36], aromatic-antiaromatic conversion [20], and photothermal therapy [25]. Although ligand-

* Corresponding authors.
E-mail addresses: wufan@nnu.edu.cn (F. Wu), zshen@nju.edu.cn (Z. Shen).

https://doi.org/10.1016/j.cclet.2024.110292
1001-8417/

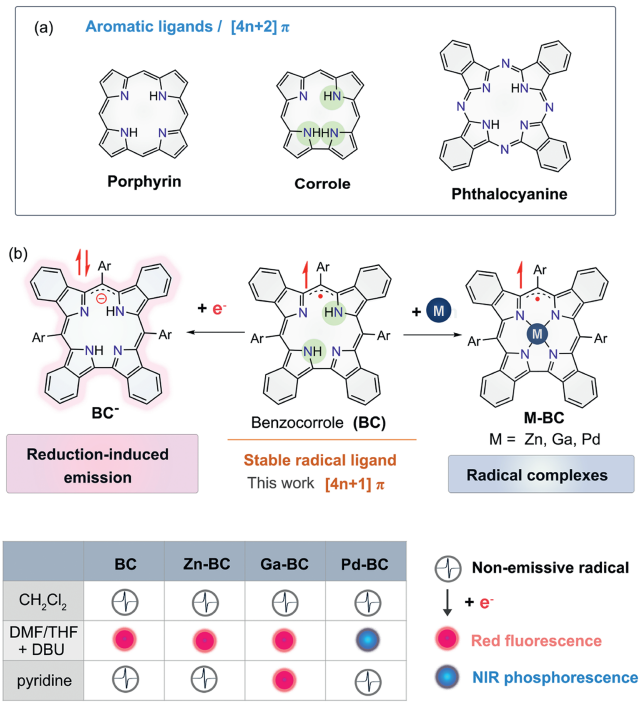

Fig. 1. (a) Structures of free-base aromatic porphyrin, corrole, and phthalocyanine. (b) Structure of the free-base benzocorrole radical and schematic of its coordination performance and reduction-induced luminescence.

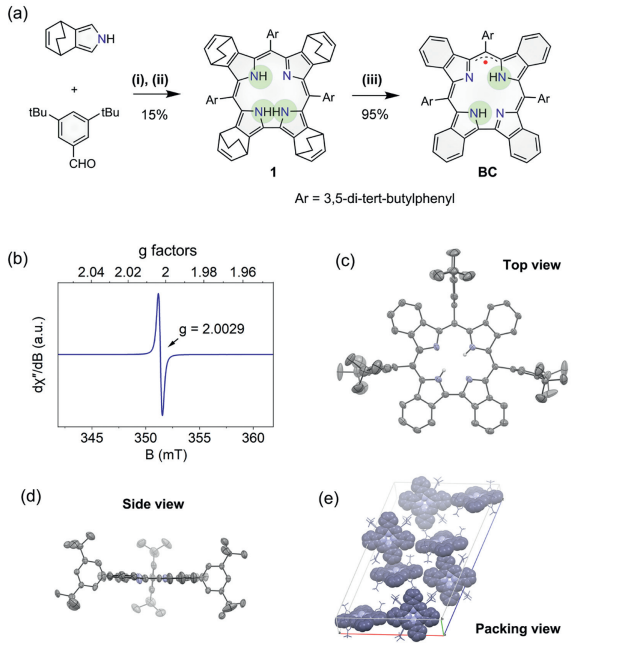

Fig. 2. (a) Synthesis of **BC**: (i) CH_3OH, H_2O, HCl, r.t.; (ii) $CHCl_3$, *p*-chloranil, reflux; (iii) 250 °C, *in vacuo*. (b) ESR spectrum of **BC** in CH_2Cl_2. (c) Top and (d) side view of the single-crystal structure of **BC** with thermal ellipsoids at 30% probability. (e) Packing view of **BC** with space-fill representation.

noninnocence was commonly found in metallocorroles, the synthesis of metal-free corrole radicals remained difficult, and Bröring *et al.* reported the first and only such free monoradical that was stabilized by *β*-chlorination [15]. It is still desirable to develop stable free-base corrole radicals for controllable coordination to create a variety of radical complexes with unique features.

In this work, we report a free-base benzocorrole (**BC**) that is highly stable in its neutral radical state at ambient conditions (Fig. 1b). **BC** consists of elements C, N, and H only, and contains two inner NHs. As a radical ligand, **BC** demonstrates easy coordination with both divalent and trivalent metal ions (Zn(II), Pd(II), and Ga(III)), and prefers to stabilize the complexes in their radical states. Red fluorescence or near-infrared phosphorescence could be activated on **BC** and its complexes *via* ligand reduction to aromatic anions under various treatments.

The benzo-fused **BC** was prepared using the *retro*-Diels-Alder approach [40]. The bicyclo[2.2.2]octadiene-fused 3*H*-corrole **1** was newly synthesized as a diastereomeric mixture *via* the direct acid-catalyzed condensation between 4,7-dihydro-4,7-ethano-2*H*-isoindole and 3,5-di–*tert*-butylbenzaldehyde in a 3:1 (v:v) methanol-water mixture solvent, followed by the oxidative cyclization by *p*-chloranil in chloroform. Heating solid **1** at 250 °C *in vacuo* eliminated its ethylene bridges and afforded radical **BC** spontaneously (Fig. 2a). The high-resolution ESI mass spectrometry for **BC** provided the exact mass at $m/z = 1061.6427$ consistent with a 2H formula $C_{77}H_{81}N_4$ (m/z 1061.6456) (Fig. S2 in Supporting information). Compound **1** was ^{1}H NMR active, indicative of its closed-shell character. In contrast, **BC** was nearly ^{1}H NMR silent, and only broad signals of *tert*–butyl protons of **BC** could be found (Fig. S15 in Supporting information). The electron spin resonance (ESR) measurement of **BC** provided an intense and sharp peak at $g = 2.0029$, clearly indicating its free organic radical character (Fig. 2b). The toluene solution of **BC** stored at ambient conditions exhibited unchanged absorption during 30-day monitoring, indicative of its intriguing stability (Fig. S25 in Supporting information).

Single crystals of **BC** were obtained from the slow diffusion of methanol into its chloroform solution and analyzed by X-ray diffraction (Figs. 2c-e). The structure of **BC** contains only two NH moieties with *trans* arrangement. Compared to 3*H*-corroles [41-43], the benzocorrole plane of **BC** demonstrates higher planarity with a mean plane deviation of only 0.056 Å due to smaller steric repulsion within the inner cavity. The amino-type pyrroles of **BC** have wider C_a-N-C_a angles (111.74° and 112.45°) than the imino-type pyrroles (109.22° and 109.74°), but imino-type pyrroles have more significant long-and-short alternation in C_α-N bond lengths (Table S3 in Supporting information). The three *meso*–aryl groups are nearly perpendicular to the corrole plane. The directly linked C_α-C_α bond length is 1.395(6) Å, which is significantly shorter than those of the reported free-base corroles ranging between 1.41 Å and 1.44 Å [15,41-43]. There is no close intermolecular stacking observed owing to the bulky 3,5–*tert*–butyl–phenyl groups.

Cyclic voltammetry and differential pulse voltammetry of **BC** reveal its reversible redox properties with oxidation peaks at $E_{ox1} = -0.12$ V, $E_{ox2} = 0.71$ V, and a reduction peak at $E_{red1} = -0.65$ V (*vs.* Fc/Fc^+) (Fig. 3a). There is no protonation-deprotonation observed during the redox processes. The gap between E_{ox1} and E_{red1} is only 0.53 V, which is typical for a free π-radical and significantly lower than the approximately 2 V gaps found in 18 π porphyrins and corroles [44,45].

The absorption spectrum of corrole **1** displays a sharp Soret band at 415 nm in CH_2Cl_2, with its emission spectrum showing a fluorescence band peaking at 654 nm (Fig. 3b). Comparatively, **BC** is fluorescence-silent in CH_2Cl_2, and exhibits an intense red-shifted absorption band at 454 nm and several weak broad bands in the range of 500–750 nm. **BC** was loaded into water-soluble nanoparticles (**BC–NPs**) by mixing with amphiphilic polymer DSPE-PEG, which exhibited near identical absorption in water as in CH_2Cl_2 and toluene. The solution color of **BC** in CH_2Cl_2 was light green and rapidly changed to pink upon HCl addition (Fig. 3c), and by adding TEA, the original color was reversibly recovered. Stepwise titration of **BC** by adding HCl incrementally revealed spectral changes with unchanged isobestic points, thus a one-step dipro-

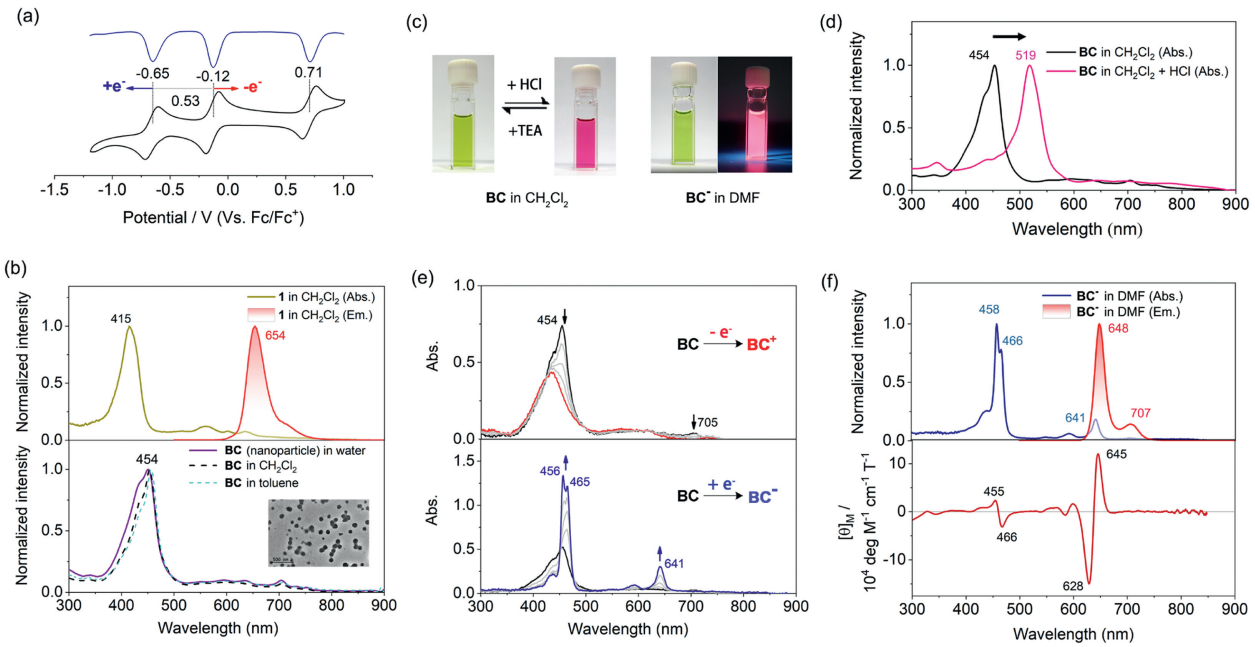

Fig. 3. (a) Electrochemical measurements of **BC** in CH_2Cl_2. (b) Absorption and fluorescence spectra of **1** in CH_2Cl_2 (λ_{ex} = 415 nm), and absorption spectra of **BC** in various solvents. (c) Images of **BC** solutions displaying the color change upon protonation and the fluorescence after reduction. (d) Absorption spectral change of **BC** upon adding HCl in the CH_2Cl_2 solution. (e) Absorption spectral changes of **BC** during oxidation and reduction recorded by spectroelectrochemistry. (f) Absorption, fluorescence (λ_{ex} = 458 nm), and MCD spectra of **BC**$^-$ in DMF (10 μmol/L, 3 mL) upon adding DBU (0.5 μL).

tonation process forming $[\mathbf{H_2BC}]^{2+}$ is purposed (Fig. S16 in Supporting information). The optimized structure of $[\mathbf{H_2BC}]^{2+}$ is highly saddle-distorted owing to the steric effect of the four inner pyrrole N-H protons. Such distortion is commonly observed in other tetrapyrrolic macrocycles that are fully protonated [46]. The absorbance maxima of $[\mathbf{H_2BC}]^{2+}$ shifts to 519 nm (Fig. 3d). The notable redshift is verified by TD-DFT calculations. The detailed compositions of the electronic transitions of $[\mathbf{H_2BC}]^{2+}$ are presented in Table S8 (Supporting information). Similar protonation-induced bathochromic shifts of absorption bands have also been observed in aromatic porphyrins and phthalocyanines [47].

The redox behaviors of **BC** associated with absorption changes were further investigated using thin-layer spectroelectrochemistry (Fig. 3e). **BC** was gradually oxidized to its cation **BC**$^+$ and reduced to anion **BC**$^-$ by shifting the applying potential positively and negatively, respectively. Isobestic points were observed on the spectral change, indicating no side reactions occurred during the redox processes. The band at 454 nm gradually decreases from **BC** to **BC**$^+$, corresponding to the conjugation change from $[4n+1]$ to $[4n]$ π. In contrast, aromatic characteristic Soret bands at 456 and 465 nm, as well as the Q band at 641 nm, intensify from **BC** to **BC**$^-$, indicating the formation of a $[4n+2]$ π system after reduction.

After adding trace 1,8-diazabicyclo[5.4.0]undec–7-ene (DBU) into the DMF solution of **BC**, the same spectral change as the reduction in spectroelectrochemistry was observed, indicating the formation of anion **BC**$^-$ (Fig. 3f). The Soret band splitting of **BC**$^-$ reflects the x and y polarizations (Table S7 in Supporting information) [48]. The chemical reduction also occurred by using THF, CH_3CN and DMSO as solvents or hydrazine, $NaBH_4$ and $SnCl_2$ as reductant (Figs. S18–S24 in Supporting information). The DMF solution of **BC**$^-$ exhibits red fluorescence, with a maximum at 648 nm and a shoulder at 707 nm in its emission spectrum. DBU has been used as a reductant in a few reactions, including the reduction of a nickel corrole radical [21,49-52]. We assume that there is a direct electron transfer from DBU to the corrole radical. forming a DBU radical that is easily quenched (Fig. S13 in Supporting information). The Hückel aromaticity of **BC**$^-$ was identified by magnetic circular dichroism (MCD) spectroscopy [53]. The coupled intense MCD Faraday B terms with a +/- sign at 645 and 628 nm in ascending energy are assigned to the Q bands of 18 π aromatic porphyrinoids, corresponding to an angular orbital momentum change of ±9. The weak MCD signals with a −/+ sign at 466 and 455 nm are ascribed to the angular orbital momentum change of ±1.

Density functional theory (DFT) calculations (B3LYP) were performed on **BC** and its redox ions (*tert*–butyl groups omitted). Two common 18 π aromatic free-base porphyrinoids, 5,10,15-triphenylcorrole (**TPC**) and 5,10,15,20-tetraphenylporphyrin (**TPP**) were also calculated for comparison. The bond lengths of DFT-optimized **BC** show good consistency with those obtained from the single-crystal structure (Fig. S28 in Supporting information). Free-base porphyrinoids exhibit tautomerism with core-hydrogen alteration [54,55], and the *trans*-NH state of **BC** is preferred with lower energy than the possible *cis*-NH tautomers (Fig. S44 in Supporting information). The spin density of **BC** exhibits very small distribution on peripheral-benzo- and *meso*–carbons, but large coefficients on the pyrrolic carbons (Fig. 4a). The molecular orbital (MO) energy level diagram indicates that **BC** exhibits better one-electron donating and accepting capabilities in comparison to **TPC** and **TPP** (Fig. 4a). Both the a_2-type lowest singly unoccupied MO (SUMO) and highest singly occupied MO (SOMO) of **BC** closely resemble the distribution of its spin density (Fig. S36 in Supporting information) [56]. Notably, the SUMO of **BC** (−3.28 eV) is more than 1 eV lower than the lowest (doubly) unoccupied MO (LUMO) of **TPC** (−2.12 eV) and **TPP** (−2.21 eV), indicating the strong electron-accepting ability of **BC** that facilitates electron pairing. Thus, the electron-transfer process could easily occur on **BC** upon adding the strong Lewis base DBU. The SOMO-SUMO gap of **BC** (1.08 eV), which is much smaller than the highest (doubly) occupied MO (HOMO)-LUMO gaps of **TPC** and **TPP**. Upon a one-electron reduction, the HOMO-LUMO gap of **BC**$^-$ is determined to be 2.44 eV, a value that closely resembles that of **TPC** (2.47 eV) (Fig. 4b). The solvent effect on the stabilization of the anion of **BC** was further evaluated by employing SMD solvent models in the calculations. The HOMO and LUMO energy levels, as well

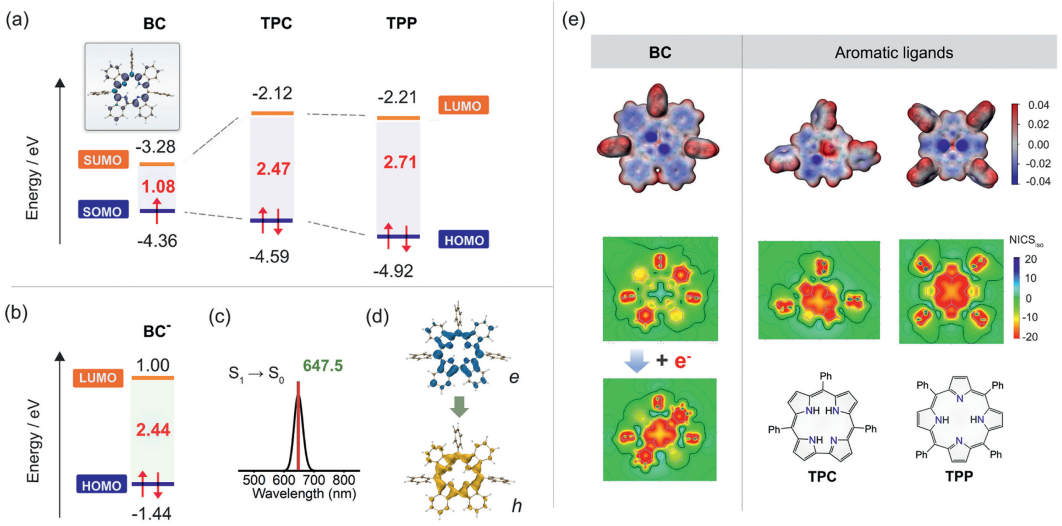

Fig. 4. (a, b) Frontier molecular orbital diagrams of **BC**, **TPC**, **TPP**, and **BC**$^-$, with the spin density map of **BC**. (c) TD-DFT simulated emission spectra of **BC**$^-$. (d) The electron (blue) and hole (yellow) distribution of the S_1 excited state on **BC**$^-$. (e) Molecular electrostatic potential and ICSS maps (1 Å above the XY plane) of **BC, TPC**, and **TPP**.

as the total energy of **BC**$^-$ in DMF, are significantly lower than those in toluene and gas phase, whereas their HOMO-LOMO gaps remain consistent (Fig. S43 in Supporting information). The time-dependent DFT (TD-DFT) calculations (B3LYP) nicely reproduce the absorption spectra of **BC**, **BC**$^+$, and **BC**$^-$, as well as the protonated **[H_2BC]$^{2+}$** (Figs. S49-S51, S56 in Supporting information). The calculated Q and Soret bands of **BC**$^-$ completely originate from its frontier four orbitals with $M_L = \pm 4$ and ± 5 (Table S7). The S_1 state of **BC**$^-$ was optimized, predicting a fluorescence band at 647.5 nm corresponding to the $S_1 \rightarrow S_0$ transition, which exactly matched the experimental finding at 648 nm (Fig. 4c). The electron and hole distributions on the S_1 state of **BC**$^-$ were analyzed by Multiwfn, revealing no spatial separation of the π-excitation (Fig. 4d) [47,57]. The Sr index, which quantifies the degree of electron-hole overlap, exhibits a value of 0.94 within the range of 0 to 1, suggesting the S_1 state of **BC**$^-$ is a locally-excited (LE) state.

DFT calculations were also performed on a variety of inner-3NH corroles with the same phenyl substituents at *meso* positions, including **TPC**, dibenzo-fused **DBC-3H**, tetrabenzo-fused **TBC-3H**, and octacarboxymethyl-substituted tetrabenzo-fused **OCTBC-3H**, to address the reason for the energy level and vertical ionization potential due to the π-extension (Table S5 in Supporting information). This indicates that it is the most unstable among the four and may tends to lose one electron and one proton under ambient conditions [13], resulting in the generation of a neutral radical.

Electrostatic potential (ESP) and Iso-chemical shielding surface (ICSS) calculations [58,59] were conducted on **BC**, **TPC**, and **TPP**, using their optimized structures (Fig. 4e). The ESP maps show that the central coordination atmosphere of **BC** is closer to that of **TPP** rather than **TPC**. **BC** has a high concentration of negative charges (blue) surrounding its two imine N atoms, indicating its Lewis base nature, which allows for further protonation or coordination. In contrast, **TPC** has significant positive charge (red) on the amine N–H, which is located opposite the negatively charged imine N atom, indicating that **TPC** is more acidic than **TPP** and **BC** [60]. The ICSS maps clearly show that both **TPC** and **TPP** are typically aromatic with the shielded region depicted in red and yellow. The nonaromatic character of **BC** is revealed by the green-cyan region with close-to-zero nucleus-independent chemical shifts (NICS) values inside the corrole ring [61]. The one-electron reduced anion **BC**$^-$ changes to aromatic, exhibiting an inner shielding area similar to neutral **TPC** and **TPP**. The NICS(1) values of **BC**$^-$, **TPC,** and **TPP** at the molecular center are −11.6, −11.3, and −13.3 ppm, respectively. The induced ring currents calculated by anisotropy of the induced current density are clockwise for **BC**$^-$, and anticlockwise for **BC**$^+$, but interrupted on the *meso* carbons of **BC** (Fig. S57 in Supporting information) [62].

The zinc, gallium, and palladium complexes of **BC** were synthesized (Fig. 5a), and all were identified as π-radicals by their sharp single-line ESR signals and spin density maps with near-zero density on central metals (Figs. S28 and S44 in Supporting information). The direct insertion of Zn(II) into 3*H*-corrole was difficult, which easily led to ring degradation [21,63]. Treating **BC** with zinc acetate in pyridine under reflux afforded stable Zn(II) complex **Zn-BC** in high yield. Ga(III) corroles were typically fluorescent molecules with axial pyridine coordination and have shown good tumor imaging and therapeutic performance [64-66]. Intriguingly, treating **BC** with $GaCl_3$ resulted in the formation of non-emitting, chloride-ligated radical **Ga-BC**, as evidenced by the single-crystal X-ray diffraction. Such radical could only be obtained by treating common aromatic gallium corroles with the additional chemical oxidant $N(4\text{-}BrC_6H_4)_3SbCl_6$ [67]. The five-coordinate Ga(III) center in **Ga-BC** has a distorted square pyramidal geometry. The Ga(III) ion is 0.487 Å above the 4 N plane, and the Ga-Cl length is 2.2208(17)Å. By adding pyridine incrementally into the toluene solution of **Ga-BC**, the fluorescence appears and gradually enhances at 637 and 700 nm (Fig. 5b), corresponding to its ligand reduction to aromatic anion. However, the reduction was not observed for **BC**, **Zn-BC**, and **Pd-BC** in pure pyridine. The mass spectrum shows that the axial chloride of **Ga-BC** could be substituted by treating it with excess pyridine (Fig. S12 in Supporting information), which may facilitate ligand reduction. The palladium insertion of 3*H*-corrole could afford a closed-shell anionic complex accompanied by a counterion [68]. A neutral palladium radical complex **Pd-BC** was synthesized for the first time *via* the reflux of **BC** and $Pd(OAc)_2$ in pyridine. Unlike **Ga-BC**, the single-crystal structure of **Pd-BC** reveals no axial ligand and the Pd(II) ion perfectly lies on the highly planar corrole plane. After adding DBU into the DMF solution of **Pd-BC**, the appearance of sharp B and Q bands indicates the formation of anion **Pd-BC**$^-$ (Fig. 5c). Interestingly, **Pd-BC**$^-$ displays near-infrared phosphorescence in the anoxic solution at room temperature owing to the promoted intersystem crossing (ISC) to triplet by palladium. The long-lived emission shows a peak at 930 nm with a microsecond-level lifetime (9.82 μs) and extends beyond 1100 nm, exhibiting a "mega" shift of 306 nm relative to the lowest energy Q band. The quantum yields

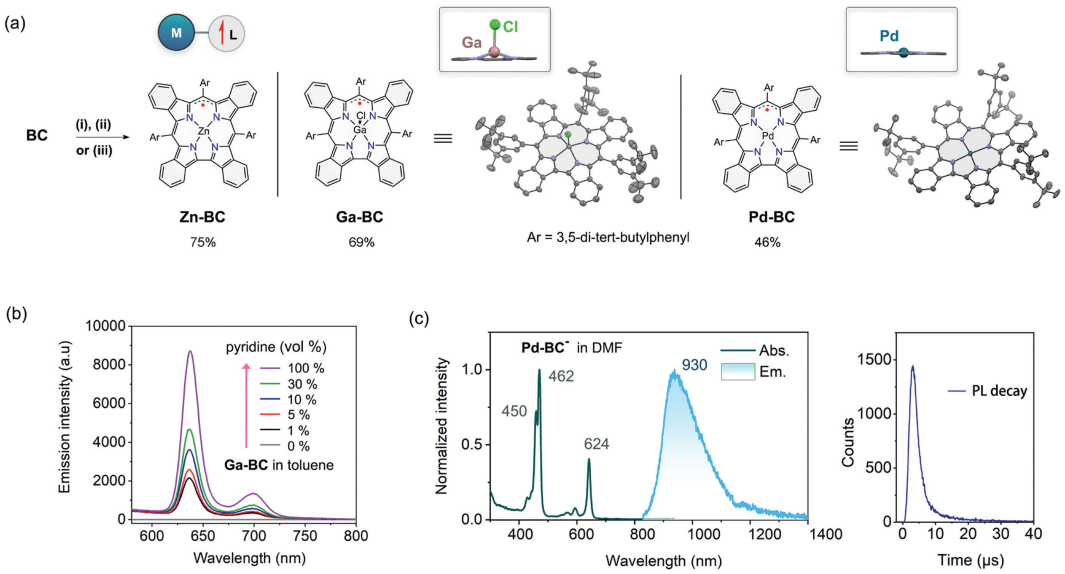

Fig. 5. (a) Synthesis and chemical structures of the radical complexes. (i) **Zn-BC**: $Zn(OAc)_2{\cdot}2H_2O$, pyridine, reflux; (ii) **Ga-BC**: $GaCl_3$, pyridine, reflux; (iii) **Pd-BC**: $Pd(OAc)_2$, pyridine, reflux. Single-crystal structures of **Ga-BC** and **Pd-BC** are presented (thermal ellipsoids at 30% probability) with central coordination structures highlighted. (b) Fluorescence spectra of **Ga-BC** in toluene as a function of the volume proportion of the added pyridine ($\lambda_{ex} = 467$ nm). (c) Absorption and emission spectra, and time-resolved photoluminescence (PL) decay curve of **Pd-BC**$^-$ in deaerated DMF upon adding DBU ($\lambda_{ex} = 624$ nm).

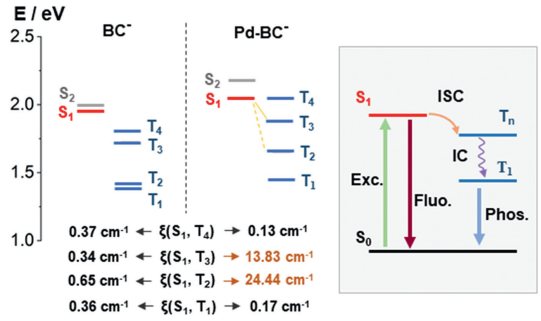

Fig. 6. Schematic diagram of the calculated energy gaps, spin-orbital coupling constants between S_1 and T_n ($n = 1$–4), and proposed energy transfer processes for fluorescence (Fluo.) and phosphorescence (Phos.).

and lifetimes of all reduced compounds are listed in Table S4 (Supporting information). The electrochemical measurements were performed on the complexes in CH_2Cl_2 (Fig. S31 in Supporting information). The difference in potential between E_{ox1} and E_{red1} is 0.49 V for **Zn-BC**, 0.59 V for **Ga-BC**, and 0.46 V for **Pd-BC**. These small gaps indicate the radical nature of the complexes.

To get a better understanding of the room-temperature phosphorescence caused by Pd coordination, the excited-state energy gaps, and spin-orbit coupling matrix elements (SOCME) between singlet state S_1 and triplet states T_n were further calculated for **BC**$^-$ and **Pd-BC**$^-$ (B3LYP) (Fig. 6) [69,70]. **BC**$^-$ exhibits four triplet states, and **Pd-BC**$^-$ exhibits three triplet states that are located below their respective S_1 state. The T_4 state of **Pd-BC**$^-$ has nearly the same energy as its S_1 state. **BC** and **Pd-BC**$^-$ have large S_1-T_1 gaps ($\Delta E_{S1\text{-}T1}$) of 0.58 eV and 0.60 eV, respectively, while their T_3 and T_4 states have small S_1-T_n gaps (<0.3 eV) that facilitate the ISC processes. All the S_1-T_n ($n = 1$–4) SOCMEs of **BC** are smaller than 0.65 cm^{-1}. For **Pd-BC**$^-$, although the S_1-T_1 and S_1-T_4 SOCMEs are minor (0.17 and 0.13 cm^{-1}, respectively), the S_1-T_2 and S_1-T_3 SOCMEs exhibit significant values of 24.44 and13.83 cm^{-1}, respectively. The ISC process is supposed to efficiently take place in the $S_1 \rightarrow T_3$ channel of **Pd-BC**$^-$ due to the narrow energy gap ($\Delta E_{S1\text{-}T3} = 0.17$ eV) and large SOCME. The higher excited triplet states T_n ($n > 1$) can undergo fast internal conversion (IC) to T_1, subsequently deactivate to the ground state S_0 and emit phosphorescence [71].

In summary, we have prepared a free-base benzocorrole radical **BC** and its various radical complexes, which were fully studied by crystallographic analysis, spectroscopic measurements, and theoretical calculations. The protonation at the inner imines of **BC** largely red-shifted its main absorption band. The fluorescence turn-on response of **BC** was discovered under the mild reducing atmosphere, corresponding to a reductive conversion to its aromatic anion. The Zn(II), Pd(II), and Ga(III) complexes of **BC** are all stable radicals and readily reduced to their emissive anions in a manner similar to **BC**. **Ga-BC** was ligated by an axial chloride, which could be replaced by pyridine accompanied by enhanced fluorescence. The anion of **Pd-BC** exhibits NIR phosphorescence beyond 900 nm at room temperature. The reduction-driven luminescence of radicals offers their potential applications in responsive imaging. This radical ligand will be used to produce new complexes with tunable redox, magnetic and emissive properties, thus broadening the application of functional radical materials.

Declaration of competing interest

The authors declare that they have no known competing financial interests or personal relationships that could have appeared to influence the work reported in this paper.

CRediT authorship contribution statement

Pengfei Li: Writing – original draft, Validation, Methodology, Investigation, Formal analysis, Data curation, Conceptualization. **Chulin Qu:** Writing – review & editing, Investigation, Formal analysis, Data curation. **Fan Wu:** Writing – review & editing, Writing – original draft, Methodology, Funding acquisition, Conceptualization. **Hu Gao:** Methodology, Investigation. **Chengyan Zhao:** Investigation, Formal analysis, Data curation. **Yue Zhao:** Visualization, Software, Resources, Methodology, Data curation. **Zhen Shen:** Writing – review & editing, Resources, Project administration, Funding acquisition, Conceptualization.

Acknowledgments

This work was supported by the National Natural Science Foundation of China (Nos. 22271140, 22071103, and 22371118). The theoretical calculations are performed using the supercomputing resources at the High-Performance Computing Center of Nanjing University.

Supplementary materials

Supplementary material associated with this article can be found, in the online version, at doi:10.1016/j.cclet.2024.110292.

References

[1] Z.X. Chen, Y. Li, F. Huang, Chem 7 (2021) 288–332.
[2] L. Ji, J. Shi, J. Wei, et al., Adv. Mater. 32 (2020) 1908015.
[3] I. Ratera, J. Veciana, Chem. Soc. Rev. 41 (2012) 303–349.
[4] D. Shimizu, A. Osuka, Chem. Sci. 9 (2018) 1408–1423.
[5] D. Shimizu, J. Oh, K. Furukawa, et al., Angew. Chem. Int. Ed. 54 (2015) 6613–6617.
[6] W. Deng, Y. Liu, D. Shimizu, et al., Chem. Eur. J. 29 (2023) e202203484.
[7] T. Yoshida, W. Zhou, T. Furuyama, et al., J. Am. Chem. Soc. 137 (2015) 9258–9261.
[8] D. Shimizu, K. Fujimoto, A. Osuka, Angew. Chem. Int. Ed. 57 (2018) 9434–9438.
[9] N. Fukui, W. Cha, D. Shimizu, et al., Chem. Sci. 8 (2017) 189–199.
[10] X.-S. Ke, Y. Hong, P. Tu, et al., J. Am. Chem. Soc. 139 (2017) 15232–15238.
[11] J. Shen, J. Shao, Ou Z, et al., Inorg. Chem. 45 (2006) 2251–2265.
[12] Y. Yamamoto, A. Yamamoto, Shin-ya Furuta, et al., J. Am. Chem. Soc. 127 (2005) 14540–14541.
[13] Y. Yamamoto, Y. Hirata, M. Kodama, et al., J. Am. Chem. Soc. 132 (2010) 12627–12638.
[14] D. Shimizu, J. Oh, K. Furukawa, et al., J. Am. Chem. Soc. 137 (2015) 15584–15594.
[15] P. Schweyen, K. Brandhorst, R. Wicht, et al., Angew. Chem. Int. Ed. 54 (2015) 8213–8216.
[16] S. Hiroto, H. Shinokubo, A. Osuka, J. Am. Chem. Soc. 128 (2006) 6568–6569.
[17] S. Ooi, D. Shimizu, K. Furukawa, et al., Angew. Chem. Int. Ed. 57 (2018) 14916–14920.
[18] S. Ooi, B. Adinarayana, D. Shimizu, et al., Angew. Chem. Int. Ed. 59 (2020) 9423–9427.
[19] A. Ghosh, Chem. Rev. 117 (2017) 3798–3881.
[20] H. Gao, F. Wu, Y. Zhao, et al., J. Am. Chem. Soc. 144 (2022) 3458–3467.
[21] M.L. Naitana, W.R. Osterloh, L. Di Zazzo, et al., Inorg. Chem. 61 (2022) 17790–17803.
[22] C.M. Lemon, M. Huynh, A.G. Maher, et al., Angew. Chem. Int. Ed. 55 (2016) 2176–2180.
[23] A.B. Alemayehu, H. Vazquez-Lima, C.M. Beavers, et al., Chem. Commun. 50 (2014) 11093–11096.
[24] R.D. Teo, J.Y. Hwang, J. Termini, et al., Chem. Rev. 117 (2017) 2711–2729.
[25] H. Gao, X. Zhi, F. Wu, et al., Angew. Chem. Int. Ed. 62 (2023) e202309208.
[26] L. Shi, H.Y. Liu, L.P. Si, et al., Chin. Chem. Lett. 21 (2010) 373–375.
[27] H. Shi, R. Liang, D.L. Phillips, et al., J. Am. Chem. Soc. 144 (2022) 7588–7593.
[28] Q.-C. Chen, S. Fite, N. Fridman, et al., ACS Catal. 12 (2022) 4310–4317.
[29] N.C. Ng, M.H.R. Mahmood, H.Y. Liu, et al., Chin. Chem. Lett. 25 (2014) 571–574.
[30] L. Yu, Q. Wang, L. Dai, et al., Chin. Chem. Lett. 24 (2013) 447–449.
[31] C. Wu, X. Li, M. Shao, et al., Chin. Chem. Lett. 33 (2022) 4559–4562.
[32] Q. Zhang, Y. Wang, Y. Wang, et al., Chin. Chem. Lett. 32 (2021) 3807–3810.
[33] Y. Zhang, K. Ren, L. Wang, et al., Chin. Chem. Lett. 33 (2022) 33–60.
[34] F. Wu, J. Liu, P. Mishra, et al., Nat. Commun. 6 (2015) 7547.
[35] J. Xu, L. Zhu, H. Gao, et al., Angew. Chem. Int. Ed. 60 (2021) 11702–11706.
[36] F. Wu, H. Gao, Y. Zhao, et al., Chin. Chem. Lett. 34 (2023) 107994.
[37] C. Yu, H. Xiao, H. Lu, et al., Chin. Chem. Lett. 35 (2024) 108883.
[38] G. Pomarico, S. Nardis, R. Paolesse, et al., J. Org. Chem. 76 (2011) 3765–3773.
[39] G. Pomarico, S. Nardis, M.L. Naitana, et al., Inorg. Chem. 52 (2013) 4061–4070.
[40] S. Ito, T. Murashima, N. Ono, et al., Chem. Commun. (1998) 1661–1662.
[41] Z. Gross, N. Galili, L. Simkhovich, et al., Org. Lett. 1 (1999) 599–602.
[42] T. Ding, J.D. Harvey, C.J. Ziegler, J. Porphyr. Phthalocyanines 09 (2005) 22–27.
[43] J. Capar, J. Conradie, C.M. Beavers, et al., J. Phys. Chem. 119 (2015) 3452–3457.
[44] Y. Fang, Z. Ou, K.M. Kadish, Chem. Rev. 117 (2017) 3377–3419.
[45] Y. Fang, M.O. Senge, E. Van Caemelbecke, et al., Inorg. Chem. 53 (2014) 10772–10778.
[46] J. Gaíate-Morales, F. Tham, C. Reed, et al., Inorg. Chem. 46 (2007) 1514–1516.
[47] S. Fukuzumi, T. Honda, T. Kojima, Coord. Chem. Rev. 256 (2012) 2488–2502.
[48] C.M. Lemon, R.L. Halbach, M. Huynh, et al., Inorg. Chem. 54 (2015) 2713–2725.
[49] T. Naito, A. saito, M. Ueda, et al., Heterocycles 65 (2005) 1857–1869.
[50] D.Y. Jeong, D.S. Lee, H.L. Lee, et al., ACS Catal. 12 (2022) 6047–6059.
[51] S. Xu, F. Yang, H. Fan, et al., New J. Chem. 46 (2022) 9994–9998.
[52] D. Shen, T. Ren, Z. Luo, et al., Org. Biomol. Chem. 21 (2023) 4955–4961.
[53] J. Mack, M.J. Stillman, N. Kobayashi, Coord. Chem. Rev. 251 (2007) 429–453.
[54] J. Helaja, M. Stapelbroek-Mo¨llmann, I. Kilpela¨inen, et al., J. Org. Chem. 65 (2000) 3700–3707.
[55] A. Mahammed, J.J. Weaver, H.B. Gray, et al., Tetrahedron Lett. 44 (2003) 2077–2079.
[56] A. Ghosh, T. Wondimagegn, A.B.J. Parusel, J. Am. Chem. Soc. 122 (2000) 5100–5104.
[57] Z. Liu, T. Lu, Q. Chen, Carbon 165 (2020) 461–467.
[58] S. Klod, E. Kleinpeter, J. Chem. Soc., Perkin Trans. 2. 10 (2001) 1893–1898.
[59] T. Lu, F. Chen, J. Comput. Chem. 33 (2012) 580–592.
[60] A. Mahammed, J.J. Weaver, H.B. Gray, et al., Tetrahedron Lett. 44 (2003) 2077–2079.
[61] Z. Chen, C. Wannere, C. Corminboeuf, et al., Chem. Rev. 105 (2005) 3842–3888.
[62] D. Geuenich, K. Hess, F. Köhler, et al., Chem. Rev. 105 (2005) 3758–3772.
[63] I. Aviv-Harel, Z. Gross, Coord. Chem. Rev. 255 (2011) 717–736.
[64] M. Pribisko, J. Palmer, R.H. Grubbs, et al., Proc. Natl. Acad. Sci. U. S. A. 113 (2016) E2258–E2266.
[65] L.G. Liu, Y.M. Sun, Z.Y. Liu, et al., Inorg. Chem. 60 (2021) 2234–2245.
[66] J. Bendix, I.J. Dmochowski, H.B. Gray, et al., Angew. Chem. Int. Ed. 39 (2000) 4048–4051.
[67] B. Basumatary, J. Rai, R.V.R. Reddy, et al., Chem. Eur. J. 23 (2017) 17458–17462.
[68] Q.C. Chen, N. Fridman, Y. Diskin-Posner, et al., Chem. Eur. J. 26 (2020) 9481–9485.
[69] F. Neese, WIREs Comp. Mol. Sci. 2 (2011) 73–78.
[70] F. Neese, WIREs Comp. Mol. Sci. 12 (2022) e1606.
[71] W. Zhao, Z. He, B.Z. Tang, Nat. Rev. Mater. 5 (2020) 869–885.